**International Journal of Solid Materials**
Vol. 1, Issue 1, 2019, Pages 79-115
Published Online on July 20, 2019

http://jyotiacademicpress.org

# INTERFACIAL STRESSES OF BONDED SINGLE-LAP JOINTS UNDER MECHANICAL AND THERMOMECHANICAL LOADS

**XIANG-FA WU and ROBERT A. JENSON**

Department of Mechanical Engineering
North Dakota State University
Fargo, ND 58108
USA
e-mail: xiangfa.wu@ndsu.edu

## Abstract

Parameterized stress analysis of bonded joints plays a crucial role in joint design and relevant life prediction. This paper provides a refined stress-function variational method for stress analysis of single-lap joints subjected to mechanical and thermomechanical loads. In the process, two stress functions are introduced to approach the interfacial shear and normal (peeling) stresses along the bonding line. The axial stresses in the adherends are assumed to be linearly varying (i.e., following that of *classic Euler-Bernoulli beam*), while the lateral normal stress and shear stresses are determined by the stress equilibrium equations within the framework of elasticity. A set of coupled 4th-order ordinary differential equations (ODEs) of these stress functions are determined via minimizing the complementary strain energy of the joints and further solved by using eigenfunctions. The stress field based on the present model can satisfy all the traction boundary conditions (BCs), and its accuracy is validated by finite element method (FEM). Detailed numerical simulations are made to show the capability of the present semi-analytic method for accurately predicting the interfacial stresses of single-lap joints under combined

Keywords and phrases: interfacial stresses, thermal stress, single-lap joints, energy method, elasticity.

Communicated by Kazem Reza Kashyzadeh.

Received March 10, 2019; Revised March 21, 2019

mechanical loads of tension, shearing, bending, and thermomechanical loads. Detailed scaling analysis is performed to explore the dependencies of interfacial stresses upon the joint geometries and material properties of the joint. The generality of this procedure guarantees the extensibility of the present semi-analytic method to other joint systems and loading cases.

## 1. Introduction

Bonded joints are broadly integrated in various mechanical and civil structures as load transfer elements, structural transition connectors, surface repairing/reinforcing patches, and so on. Subjected to external loading or environmental temperature change, high stress concentration is triggered near the adherend ends of bonded joints due to the mismatch of material properties of the adherends across the bonding lines. The existence of high interfacial stresses at adherend ends is one of the main factors responsible for the debonding failure of joints as commonly observed in engineering practice. Therefore, accurate prediction of the debonding stresses in bonded joints is crucial to structural design and damage prediction. Due to the structural importance and geometrical complexity of bonded joints as well as the concurrence of several dissimilar materials at a localized region, the accurate stress analysis of joints has been a challenging topic in applied mechanics and structural engineering which has been attracted substantial attention in the last six decades.

Historically, Volkersen [1] first conducted the stress analysis of an adhesively bonded joint by introducing the concept of differential shear, in which the compliant adhesive layer was restrained to deform only in shear while the stiff adherends were treated as two tension bars. Goland and Reissner [2] furthered Volkersen's work and treated the adherends as slender beam segments. These two studies are generally considered as the milestone of joint stress analysis in the literature and commonly cited by many researchers. As a matter of fact, a majority of the late investigations can be traced to the pioneering studies by Volkersen [1]

and Goland and Reissner [2]. Recently, da Silva et al. [3, 4] made a detailed comparative study on a variety of analytical models of adhesively bonded joints. Among these, a few important theoretical contributions are mentioned as follows. Hart-Smith [5, 6] developed the elastoplastic strength models of adhesively bonded lap joints based on the maximum shear-strain failure criterion, which are capable of determining the load-carrying capability of the joints. Based on the classic beam theory, Erdogan and Ratwani [7] and Delale et al. [8] took into account the contribution of adherend rotation and formulated a set of governing equations to determine the debonding stresses of a variety of adhesively bonded joints including strap, lap, butt, scarf, and stepped joints. However, due to the limitation of the classic beam theory, the interfacial shear-stress predicted by all above joint models and a significant number of follow-ups cannot satisfy the free-shear stress conditions at adherend ends. In addition, treatment of the adhesive layer as a shear spring conflicts with the generalized Hooke's law of the adhesive layer. Furthermore, based on theorem of minimum complementary strain energy, Chen and Cheng [9-11] proposed an energy approach for the stress analysis of lap, butt, scarf, and tubular joints. In the case of adhesively bonded single-lap joints, a set of governing equations was obtained which consisted of two coupled 4th-order ordinary differential equations (ODEs) of two unknown axial tensile stresses. This model predicted that the peak shear-stress in the adhesive layer locates at a distance of ~20% the adherend thickness from the adherend ends, close to those predicted by detailed Finite Element Method (FEM). This method was further extended by Wu et al. [12] for stress and progressive cracking analysis of circular torsion shafts with surface coatings. In addition, with the expanding applications of joining technologies in a broad spectrum of industrial sectors, stress analysis of joints has been furthered and refined such as the extensive investigations of tubular joints [13-18] and nonlinear and high-order analysis of bonded joints [19-22], adhesive failure and debonding analysis of adhesively

bonded joints [23-32], and development of new concept joints including piezoelectric patch-based smart joints [33-36], among others. More recently, Khan et al. [37] formulated a theoretical Adhesively Bonded Joint (ABJ) model to take into account the effect of transverse shear of the ABJ adherends. In the model, the ABJ adherends are treated as Timoshenko's beams and this model was used to guide to reduce the interfacial shear and peeling stresses via material tailoring.

Besides, several recent layerwise joint models have been formulated for improved stress analysis of ABJs. For instance, Hadj-Ahmed et al. [38] formulated a layerwise ABJ model with the multi-layers of the ABJ to be modelled as a stack of Reissner plates that are coupled through the interlaminar normal and shear stresses. The governing equations of the ABJs are obtained via minimizing the strain energy of the ABJ. Diaz et al. [39] also proposed an improved layerwise ABJ model, in which the ABJ was modelled as a stack of Reissner-Mindlin plates. As a result, a set of eight governing ODEs was obtained via evoking the constitutive laws and solved to satisfy the traction BCs. This ABJ model can be well validated by FEM for free-edge interfacial stress prediction. Moreover, Yousefsani and Tahani [40, 41] provided another version of the layerwise ABJ models. In their models, the displacements of artificially divided sub-layers of an ABJ were treated as field variables, and a set of governing ODEs was obtained via minimizing the potential energy of the joint. For accurate interfacial stress prediction, 18 artificial sub-layers were used in their numerical examples. Such layerwise ABJ models were further extended for stress analysis of smart joints integrated with piezoelectric patches in their recent efforts [42].

Nevertheless, accurate stress analysis is crucial to formulation of robust joint models and the design and failure prediction of bonded joints. Though purely numerical stress analysis such as FEM can provide detailed understanding of the stress field in a specific joint, parameterized analytic and semi-analytic methods are still desired and

have their intellectual merits since they enable an explicit interpolation of the stress dependency upon the material parameters and geometries and can be conveniently used for scaling analysis. Along the vein of stress analysis of bonded joints, a reliable stress-function variational method has been proposed by Wu and his co-workers [43-46]. This method has been used successfully to determine the entire stress field of single-sided strap joints [43-46]. In the process, by introducing two unknown interfacial shear and normal stress functions, all the stress components in the joint were expressed in terms of the unknown stress functions with the axial flexural stresses to satisfy that of *Euler-Bernoulli beams* and the left shear and transverse normal stress components to satisfy the stress equilibrium equations of elasticity at the given traction boundary conditions (BCs). A set of two coupled governing ODEs was obtained through minimizing the complementary strain energy of the joint similar to those considered by Chen and Cheng [9-11] and Wu et al. [12]. This set of ODEs can be solved to satisfy all the traction BCs of the joint, and gives the stress field of the joint with improved accuracy. In this work, this method is further extended to determine the stress field of a bonded single-lap joint made of two dissimilar isotropic, linearly thermoelastic adherends. Due to loss of the structural and loading symmetry, the stress field of a single-lap joint belongs to a general case of bonded joints compared to that of a single-sided strap joint [38]. Thus, the most general solution will be derived for the general traction BCs of a bonded single-lap joint, including the combination of tensile and shear-force as well as bending moments. The present work will provide a uniform treatment of stress analysis of bonded joints subjected to mechanical and thermomechanical loads. Such treatment is useful to the study of debonding failure and fracture of bonded joints and other layered structures [46-57]. The rest of the paper is planned as follows. Section 2 presents the theoretical framework of stress-function variational method for bonded single-lap joints under the general traction BCs, including derivation of the adherend stresses in terms of the interfacial stress

functions and formulation of the set of governing ODEs. Section 3 demonstrates the present method for stress analysis of bonded single-lap joints subjected to mechanical and thermomechanical loads. Comparisons of the results with those given by FEM are made and applications of the present study are remarked. The conclusions of the present study are drawn in Section 4.

## 2. Problem Formulation and Solution

Consider a bonded single-lap joint made of two homogenous, isotropic, linearly thermoelastic adherends as illustrated in Figure 1. Both adherends of the joint are treated as slender beams to carry the overlapped length $L$ and consistent width $b$. The thicknesses of the upper and lower adherends are designated as $h_1$ and $h_2$, respectively. The coordinate systems are established as follows. The $x$-coordinate is selected from the left end of the overlap and directs along the layer neutral axis; $y_1$ and $y_2$ are the transverse coordinates with the individual origins located at the centroids of cross-section of the adherend layers, respectively. The joint is subjected to the general traction BCs of tensile force $P_0$, shear-force $V_0$, and bending moments $M_1$ and $M_2$ as illustrated in Figure 1(b); meanwhile the joint has a uniform temperature change $\Delta T$ from the reference temperature of thermal-stress-free state. Mismatch of the adherend properties across the bonding interface may induce high interfacial shear and normal (peeling) stresses at the adherend ends as sketched in Figure 1(c). Such high interfacial stresses are the main factors responsible for the failure of the bonded joint.

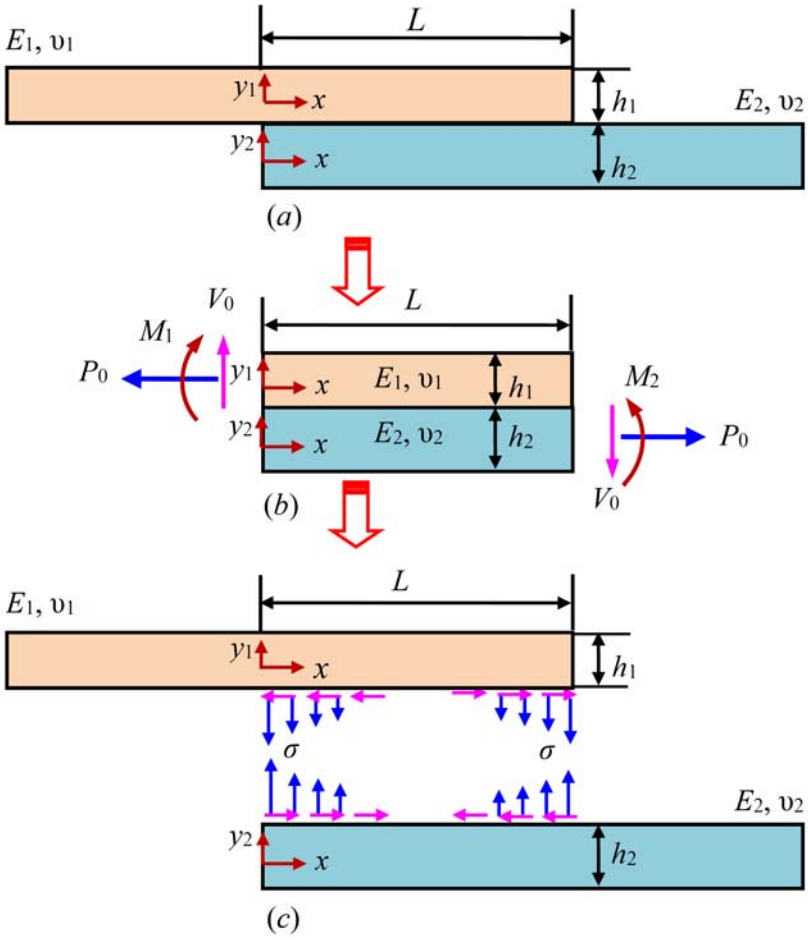


**Figure 1.** Schematic of a bonded single-lap joint: (a) the joint consists of two slender adherends, (b) free-body diagram of the joint with effective traction boundary conditions, and (c) schematic interfacial shear and normal stresses.

In engineering practice, a complicated three-dimensional (3D) stress state exists at the adherend corners of the bonded single-lap joints due to the finite width of the joint plus the mismatch of Poisson's ratios and coefficients of thermal expansion of the adherends. Stress analysis of such bonded joints usually needs detailed 3D finite element analysis

(FEA). To simplify this process, *plane-stress* and *plane-strain* states will be considered as two limiting cases of engineered bonded joints. Such treatment will greatly facilitate the understanding of the scaling properties of interfacial stresses in bonded joints with respect to the material properties and joint geometries. Besides, for the convenience of the derivation hereafter, the following notation convention will be implied such that parameters and variables with subscripts 1 and 2 are denoted to those of the upper and lower adherends, respectively. In addition, the *plane-stress* results can be conveniently converted to those of the *plane-strain* state by simply replacing the Young's moduli $E_i (i = 1, 2)$ by $E_i/(1-\upsilon_i^2)$, Poisson's ratio $\upsilon_i (i = 1, 2)$ by $\upsilon_i/(1-\upsilon_i)$, and coefficients of thermal expansion $a_i (i = 1, 2)$ by $(1+\upsilon_i)\alpha_i$.

### 2.1. Static equilibrium equations

For a single lap-joint under general loadings of tension, shearing, and bending as well as temperature change, the deformation of the joint consists of in-plane elongation and lateral deflection. Similar to our recent study of the single-sided strap joint [43-45], the adherends of joint are treated as slender *Euler-Bernoulli beams*. Free-body diagrams (FBDs) of the representative segments of the adherends are shown in Figures 2(a) and 2(b), respectively. The stress components and the corresponding stress resultants, i.e., the axial force $S_i$, shear-force $Q_i$, and bending moment $M_i$ $(i = 1, 2)$, are defined to follow the standard sign conventions designated in the elementary beam theory; however, the sign convention of the shear-stress is opposite to that defined in elasticity. For the representative segmental element of the upper adherend (see Figure 2(a)), the corresponding static equilibrium equations are

$$\sum F_x = 0 : \frac{dS_1}{dx} = -b\tau, \tag{1}$$

$$\sum F_y = 0 : \frac{dQ_1}{dx} = -b\sigma, \tag{2}$$

$$\sum M = 0 : \frac{dM_1}{dx} = Q_1 - \frac{h_1}{2}(b\tau). \tag{3}$$

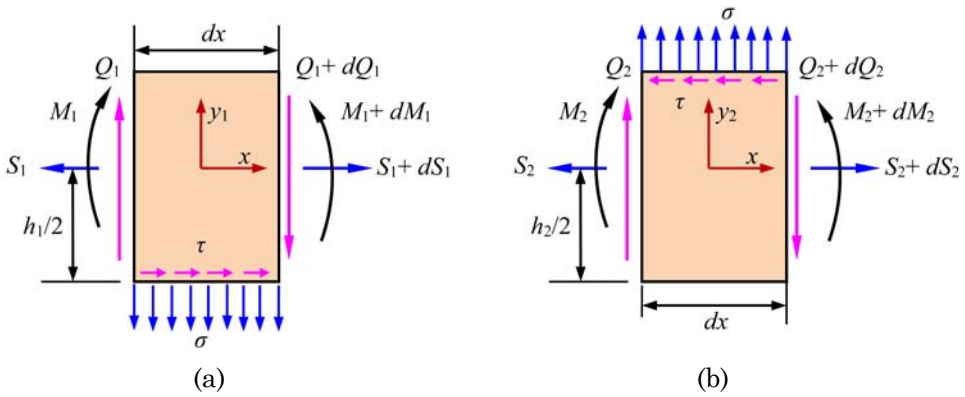


**Figure 2.** Free-body diagrams of representative segmental elements of the adherends: (a) the upper adherend and (b) the lower adherend.

The static equilibrium equations of the representative segmental element of the lower adherend (see Figure 2(b)) are

$$\sum F_x = 0 : \frac{dS_2}{dx} = b\tau, \tag{4}$$

$$\sum F_y = 0 : \frac{dQ_2}{dx} = b\sigma, \tag{5}$$

$$\sum M = 0 : \frac{dM_2}{dx} = Q_2 - \frac{h_2}{2}(b\tau). \tag{6}$$

### 2.2. Stress resultants in adherends

By adopting the procedure considered recently by the authors [37], two interfacial stress functions, i.e., the interface shear $\tau$ and interfacial normal (peeling) stress $\sigma$, are introduced as two independent functions to be determined:

$$\tau = f(x) \text{ and } \sigma = g(x). \tag{7}$$

Shear-free condition at the right and left adherend edges ($x = 0$ and $L$) requires

$$f(0) = f(L) = 0. \tag{8}$$

Traction BCs at the both adherend ends the single-lap joint are

$$S_1(0) = p_0 b h_2, \tag{9}$$

$$S_1(L) = 0, \tag{10}$$

$$Q_1(0) = t_0 b h_2, \tag{11}$$

$$Q_1(L) = 0, \tag{12}$$

$$M_1(0) = M_1 b, \tag{13}$$

$$M_1(L) = 0, \tag{14}$$

$$S_2(0) = 0, \tag{15}$$

$$S_2(L) = p_0 b h_2, \tag{16}$$

$$Q_2(0) = 0, \tag{17}$$

$$Q_2(L) = t_0 b h_2, \tag{18}$$

$$M_2(0) = 0, \tag{19}$$

$$M_2(L) = -M_2(b). \tag{20}$$

In the above, $p_0$, $t_0$, $M_1$, and $M_2$ are the average normal stress and shear-stress, and the bending moments per unit width of the joint, respectively. In general, the bending moments $M_1$ and $M_2$ can carry different values subjected to satisfaction of the moment equation, while $S_1(0) = -S_2(L)$ and $Q_2(0) = -Q_2(L)$ according to the equations of static equilibrium of the joint.

In the case of thermomechanical stress analysis of the joint due to a pure temperature change $\Delta T$, the right terms of (9), (11), (13), (16), (18), and (20) should be set as zero to satisfy the traction-free BCs. In such a case, the thermomechanical stress analysis of a single-lap joint is equivalent to that of a bi-material thermostat [43-45].

By following the similar derivations performed recently by the authors [43], all the stress resultants of the segmental elements of the upper and lower adherends can be expressed uniformly in terms of $f$ and $g$. In the upper adherend, the stress resultants are

$$S_1(x) = p_0 b h_2 - \int_0^x b f(\xi) d\xi, \tag{21}$$

$$Q_1(x) = t_0 b h_2 - b \int_0^x g(\xi) d\xi, \tag{22}$$

$$M_1(x) = M_1 b + t_0 h_2 b x - b \int_0^x \int_0^\xi g(\zeta) d\zeta d\xi - \frac{b h_1}{2} \int_0^x f(\xi) d\xi. \tag{23}$$

In the lower adherend, the stress resultants are

$$S_2(x) = b \int_0^x f(\xi) d\xi, \tag{24}$$

$$Q_2(x) = b \int_0^x g(\xi) d\xi, \tag{25}$$

$$M_2(x) = b \int_0^x \int_0^\xi g(\zeta) d\zeta d\xi - \frac{b h_2}{2} \int_0^x f(\xi) d\xi. \tag{26}$$

### 2.3. Stress components of bonded single-lap joints

#### 2.3.1. Stress components in the upper adherend

For slender adherends of the bonded single-lap joint under consideration, the axial normal stress in the upper adherend can be assumed to follow that of an *Euler-Bernoulli* beam [43-46]:

$$\sigma_{xx}^{(1)} = \frac{S_1}{bh_1} - \frac{M_1(x)y_1}{I_1} = p_1 - \frac{1}{h_1}\int_0^x f(\xi)d\xi - \frac{12y_1}{h_1^3}[M_1 + t_0h_2x$$

$$- \int_0^x \int_0^\xi g(\zeta)d\zeta d\xi\} - \frac{h_1}{2}\int_0^x f(\xi)d\xi], \tag{27}$$

where $p_1 = p_0(h_2 / h_1)$. The corresponding shear-stress $\tau_{y_1x}^{(1)}$ of the upper adherend can be determined by integrating the 2D equilibrium equation of a representative stress element:

$$\frac{\partial\sigma_{xx}^{(1)}}{\partial x} + \frac{\partial\tau_{y_1x}^{(1)}}{\partial y_1} = 0, \tag{28}$$

with respect to $y_1$ from an arbitrary location $y$ to the top surface at $y_1 = h_1/2$:

$$\int_{y_1}^{h_1/2} \frac{\partial\sigma_{xx}^{(1)}}{\partial x} dy_1 + \int_{y_1}^{h_1/2} \frac{\partial\tau_{y_1x}^{(1)}}{\partial y_1} dy_1 = 0, \tag{29}$$

which leads to

$$\tau_{y_1x}^{(1)} = -\frac{1}{h_1}[(\frac{h_1}{2} - y_1) - \frac{3}{h_1}(\frac{h_1^2}{4} - y_1^2)]f(x)$$

$$+ \frac{6}{h_1^3}(\frac{h_1^2}{4} - y_1^2)[\int_0^x g(\xi)d\xi - t_0h_2]. \tag{30}$$

In the above, the traction-free BC: $\tau_{y_1x}^{(1)}(h_1 / 2) = 0$ at the top surface of the upper adherend has been evoked. Besides, transverse normal stress $\sigma_{y_1y_1}^{(1)}$ in the upper adherend can be calculated by integrating the 2D equilibrium equation of elasticity:

$$\frac{\partial\sigma_{y_1y_1}^{(1)}}{\partial y_1} + \frac{\partial\tau_{xy_1}^{(1)}}{\partial x} = 0, \tag{31}$$

with respect to $y_1$ from an arbitrary location $y$ to the top surface of the adherend at $y_1 = h_1/2$ as

$$\int_{y_1}^{h_1/2} \frac{\partial \sigma_{y_1 y_1}^{(1)}}{\partial y_1} dy_1 + \int_{y_1}^{h_1/2} \frac{\partial \tau_{xy_1}^{(1)}}{\partial x} dy_1 = 0, \tag{32}$$

which yields

$$\sigma_{y_1 y_1}^{(1)} = -\frac{1}{h_1}\{\frac{h_1}{2}(\frac{h_1}{2} - y_1) - \frac{1}{2}(\frac{h_1^2}{4} - y_1^2) - \frac{3}{h_1}[\frac{h_1^2}{4}(\frac{h_1}{2} - y_1)$$

$$- \frac{1}{3}(\frac{h_1^3}{8} - y_1^3)]\}f'(x) + \frac{6}{h_1^3}[\frac{h_1^2}{4}(\frac{h_1}{2} - y_1) - \frac{1}{3}(\frac{h_1^3}{8} - y_1^3)]g(x). \tag{33}$$

### 2.3.2. Stress components in the lower adherend

By adopting the similar procedure in Subsection 2.3.1, the stress components in the lower adherend can be determined as

$$\sigma_{xx}^{(2)} = \frac{S_2}{bh_2} - \frac{M_2 y_2}{I_2} = \frac{1}{h_2}\int_0^x f(\xi)d\xi - \frac{12y_2}{h_2^3}[\int_0^x \int_0^\xi g(\zeta)d\zeta d\xi - \frac{h_2}{2}\int_0^x f(\xi)d\xi], \tag{34}$$

$$\tau_{y_2 x}^{(2)} = -\frac{1}{h_2}[(y_2 + \frac{h_2}{2}) + \frac{3}{h_2}(y_2^2 - \frac{h_2^2}{4})]f(x) + \frac{6}{h_2^3}(y_2^2 - \frac{h_2^2}{4})]\int_0^x g(\xi)d\xi, \tag{35}$$

$$\sigma_{y_2 y_2}^{(2)} = \{\frac{1}{h_2}[\frac{1}{2}(y_2^2 - \frac{h_2^2}{4}) + \frac{h_2}{2}(y_2 + \frac{h_2}{2})] + \frac{3}{h_2^2}[\frac{1}{3}(y_2^3 + \frac{h_2^3}{8}) - \frac{h_2^2}{4}(y_2$$

$$+ \frac{h_2}{2})]\}f'(x) - \frac{6}{h_2^3}[\frac{1}{3}(y_2^3 + \frac{h_2^3}{8}) - \frac{h_2^2}{4}(y_2 + \frac{h_2}{2})]g(x). \tag{36}$$

Compared to those obtained recently [43-46] for specific side-bonded strap joints, the stress expressions (27), (30), and (33) have taken into account the contribution of the axial normal force, shear force, and bending moment; while the stress expressions (34)-(36) of the lower adherend have the same expressions as those for single-sided strap joints due to the same traction BCs at the left end. In addition, the present stress expressions, (i.e., (27), (30), (33), and (34)-(36)) represent the most general case, which can be used for the stress determination of any bonded joints made of two adherends. The above stress approaches also indicate that the axial normal stress varies linearly across the adherends, while the statically compatible shear and transverse normal stresses vary parabolically and cubically across the adherends, respectively.

### 2.4. Governing differential equations for the interfacial stresses and solution

The theorem of minimum complementary strain energy is adopted for the stress determination of the current single-lap joints similar to those reported in the literature [9-12] and also considered in our recent studies of progressive cracking of surface coatings [12] and debonding stresses of side-bonded strap joints [37-40]. In the present case, the strain energy of the joint within the overlapped region $(0 \le x \le L)$ can be expressed as

$$U = b\int_0^L \int_{-h_1/2}^{h_1/2} \{ \frac{1}{2} [\sigma_{xx}^{(1)}\varepsilon_{xx}^{(1)} + \sigma_{yy}^{(1)}\varepsilon_{yy}^{(1)}] + \frac{1+\upsilon_1}{E_1} (\tau_{xy_1}^{(1)})^2 \} dx dy_1$$

$$+ b\int_0^L \int_{-h_2/2}^{h_2/2} \{ \frac{1}{2} [\sigma_{xx}^{(2)}\varepsilon_{xx}^{(2)} + \sigma_{yy}^{(2)}\varepsilon_{yy}^{(2)}] + \frac{1+\upsilon_1}{E_1} (\tau_{xy_2}^{(2)})^2 \} dx dy_2. \qquad (37)$$

In the above, $\varepsilon_{xx}^{(i)}$ and $\varepsilon_{yy}^{(i)}$ $(i = 1, 2)$ are respectively the axial and transverse normal strains of the adherends, which can be determined according to the generalized Hooke's law of isotropic, linearly thermoelastic solids. In the *plane-stress* state, these normal strains are

$$\varepsilon_{xx}^{(i)} = \frac{1}{E_i}\sigma_{xx}^{(i)} - \frac{\upsilon_i}{E_i}\sigma_{yy}^{(i)} + \alpha_i \Delta T, \tag{38}$$

$$\varepsilon_{yy}^{(i)} = \frac{1}{E_i}\sigma_{yy}^{(i)} - \frac{\upsilon_i}{E_i}\sigma_{xx}^{(i)} + \alpha_i \Delta T, \tag{39}$$

where $\alpha_i (i = 1, 2)$ are coefficients of thermal expansion of the adherends above and below, respectively, and $\Delta T$ is the uniform temperature change of the joint from a reference temperature of thermal-stress free state. Also, the strain energy (37) is an energy functional with respect to the interfacial stress functions $f$ and $g$. In addition, for linearly thermoelastic materials, the complementary strain energy of an elastic body is equivalent to the corresponding strain energy of this elastic body. Thus, according to theorem of minimum complementary strain energy of elastic bodies, the strain energy of the joint reaches a stationary point in the state of static equilibrium. This yields the necessary condition that variation of the strain energy (26) equals to zero [9-12, 43-46]:

$$\delta U = 0, \tag{40}$$

i.e.,

$$\begin{aligned}\delta U = b\int_0^L \int_{-h_1/2}^{h_1/2} \{ \frac{1}{2}[\sigma_{xx}^{(1)}\delta\varepsilon_{xx}^{(1)} + \delta\sigma_{xx}^{(1)}\varepsilon_{xx}^{(1)} + \sigma_{yy}^{(1)}\delta\varepsilon_{yy}^{(1)} + \delta\sigma_{yy}^{(1)}\varepsilon_{yy}^{(1)}] \\ + \frac{2(1+\upsilon_1)}{E_1}\tau_{xy_1}^{(1)}\delta\tau_{xy_1}^{(1)} \} dx dy_1 \\ + b\int_0^L \int_{-h_2/2}^{h_2/2} \{ \frac{1}{2}[\sigma_{xx}^{(2)}\delta\varepsilon_{xx}^{(2)} + \delta\sigma_{xx}^{(2)}\varepsilon_{xx}^{(2)} + \sigma_{yy}^{(2)}\delta\varepsilon_{yy}^{(2)} + \delta\sigma_{yy}^{(2)}\varepsilon_{yy}^{(2)}] \\ + \frac{2(1+\upsilon_2)}{E_2}\tau_{xy_2}^{(2)}\delta\tau_{xy_2}^{(2)} \} dx dy_2,\end{aligned} \tag{41}$$

where $\delta$ is the mathematical variational operator with respect to either $f$ or $g$.

Similar to our recent study [43-46], governing equations of the interfacial stress functions $f$ and $g$ can be extracted by substituting the stress components (27), (30), (33), and (34)-(36) and strain components (38)-(39) into (41) and performing several variational operations and mathematical simplifications. As a result, a set of two coupled 4th-order ODEs of constant coefficients can be determined:

$$A_{11}F^{(IV)}(\xi) + A_{12}G^{(IV)}(\xi) + B_{11}F^{//}(\xi) + B_{12}G^{//}(\xi) + C_{11}F(\xi) + C_{12}G(\xi) + D_1 = 0, \tag{42}$$

$$A_{12}F^{(IV)}(\xi) + A_{22}G^{(IV)}(\xi) + B_{12}F^{//}(\xi) + B_{22}G^{//}(\xi) + C_{12}F(\xi) + C_{22}G(\xi) + D_2 = 0, \tag{43}$$

where

$$F(\xi) = F(x / h_2) = -\frac{1}{p_0 h_2}\int_0^x f(\zeta)d\zeta, \tag{44}$$

$$G(\xi) = G(x / h_2) = \frac{1}{p_0 h_2^2}\int_0^x\int_0^\zeta g(\eta)d\eta d\zeta, \tag{45}$$

$$A_{11} = \frac{1}{105}(h_{12}^3 + e_{12}), \tag{46}$$

$$A_{12} = \frac{11}{210}(-h_{12}^2 + e_{12}), \tag{47}$$

$$A_{22} = \frac{13}{35}(h_{12} + e_{12}), \tag{48}$$

$$B_{11} = -\frac{4}{15}(h_{12} + e_{12}), \tag{49}$$

$$B_{12} = \frac{1}{5}[(1 - 5\upsilon_1) - (1 - 5\upsilon_2)e_{12}], \tag{50}$$

$$B_{22} = -\frac{12}{5}(h_{12}^{-1} + e_{12}), \tag{51}$$

$$C_{11} = 4(h_{12}^{-1} + e_{12}), \tag{52}$$

$$C_{12} = 6(-h_{12}^{-2} + e_{12}), \tag{53}$$

$$C_{22} = 12(h_{12}^{-3} + e_{12}), \tag{54}$$

$$D_1 = \begin{cases} h_{12}^{-1} + 6h_{12}^{-2}\left(\dfrac{M_1}{p_0 h_2^2} + \dfrac{t_0}{p_0}\xi\right) + \dfrac{1}{2}(\alpha_1 - \alpha_2)\Delta T E_1/p_0, \\ \qquad \text{(for thermomechanical loads – plane-stress state)} \\ h_{12}^{-1} + 6h_{12}^{-2}\left(\dfrac{M_1}{p_0 h_2^2} + \dfrac{t_0}{p_0}\xi\right) + \dfrac{1}{2}[\alpha_1(1+\upsilon_1) - \alpha_2(1+\upsilon_2)]\Delta T E_1/p_0, \\ \qquad \text{(for thermomechanical loads – plane-stain state)} \\ h_{12}^{-1} + 6h_{12}^{-2}\left(\dfrac{M_1}{p_0 h_2^2} + \dfrac{t_0}{p_0}\xi\right), \\ \qquad \text{(for pure mechanical load – either plane-stress or plane-stain state)} \\ \dfrac{1}{2}(\alpha_1 - \alpha_2)\Delta T E_1/p_0, \text{ (for pure thermal loads – plane-stain state)} \\ \dfrac{1}{2}[\alpha_1(1+\upsilon_1) - \alpha_2(1+\upsilon_2)]\Delta T E_1/p_0, \\ \qquad \text{(for pure thermal loads – plane-stain state)} \end{cases} \tag{55}$$

$$D_2 = \begin{cases} -12h_{12}^{-3}\left(\dfrac{M_1}{p_0 h_2^2} + \dfrac{t_0}{p_0}\xi\right), \\ \qquad \text{(for pure mechanical of thermomechanical loads)} \\ 0, \quad \text{(for pure thermal load)} \end{cases} \tag{56}$$

$$h_{12} = h_1 / h_2, \tag{57}$$

$$e_{12} = E_1 / E_2, \tag{58}$$

$$\xi = x / h_2. \tag{59}$$

The governing ODEs (42) and (43) and relations (44)-(54), (57), and (58) carry the same expressions as those obtained recently [38] for side-bonded strap joints. In fact, the governing ODEs (42) and (43) are universal for stress analysis of any joints made of two bonded adherends. In addition, the specific type of the bonded two-adherend joint specifies the expressions of (55) and (56), which are in the general case. In the special case of $t_0 = 0$, and $M_1 = p_0 h_2(h_1 + h_2)/2$, the above derivations recover those developed for side-bonded strap joints [44]. In addition, in the case of tension-free joints (e.g., pure bending, combination of bending and shearing), $h_{12}^{-1}$ in the first three expression of $D_1$ in (55) should be ignored and $p_0$ should be understood as a reference stress for dimensionless stress expressions. Moreover, the governing ODEs (42) and (43) can be utilized for the case of *plane-strain* joints by replacing $E_i$ by $E_i/(1-\upsilon_i^2)$, $\upsilon_i$ by $\upsilon_i/(1-\upsilon_i)$, and $\alpha_i$ by $(1+\upsilon_i)\alpha_i$, where $i = 1, 2$ to denote the material properties of the adherends above and below, respectively.

For the convenience of the numerical solving process, the governing ODEs (42) and (43) can be further expressed in the matrix format [44-46]:

$$[A]\{\Phi^{(IV)}\} + [B]\{\Phi''\} + [C]\{\Phi\} + \{D\} = \{0\}, \tag{60}$$

where [*A*], [*B*], and [*C*] are three $2 \times 2$ symmetric real matrices:

$$[A] = [A]^T = \begin{bmatrix} A_{11} & A_{12} \\ A_{12} & A_{22} \end{bmatrix}, \tag{61}$$

$$[B] = [B]^T = \begin{bmatrix} B_{11} & B_{12} \\ B_{12} & B_{22} \end{bmatrix}, \tag{62}$$

$$[C] = [C]^T = \begin{bmatrix} C_{11} & C_{12} \\ C_{12} & C_{22} \end{bmatrix}, \tag{63}$$

and $\{\Phi\}$, $\{D\}$, and $\{0\}$ are three vectors defined as

$$\{\Phi\} = \{F(\xi),\, G(\xi)\}^T, \tag{64}$$

$$\{D\} = \{D_1,\, D_2\}^T, \tag{65}$$

$$\{0\} = \{0,\, 0\}^T. \tag{66}$$

Similar to the solving procedure considered by Wu and his co-worker [44-46], the solution to (60) can be obtained by superimposing the general solution $\{\Psi\}$ of the corresponding homogeneous ODEs to the particular solution $\{\Phi_0\}$:

$$\{\Phi\} = \{\Psi\} + \{\Phi_0\}, \tag{67}$$

$$[A]\{\Psi^{(IV)}\} + [B]\{\Psi''\} + [C]\{\Psi\} = \{0\}, \tag{68}$$

$$\{\Phi_0\} = -\,[C]^{-1}\{D\}, \tag{69}$$

$$\frac{d}{d\xi}\{\Phi_0\} = -\,[C]^{-1}\frac{d}{d\xi}\{D\} = -\,6h_{12}^{-2}[C]^{-1}\begin{Bmatrix}1\\ \\ -\,2h_{12}^{-1}\end{Bmatrix}(t_0/p_0). \tag{70}$$

In the above, the particular solution $\{\Phi_0\}$ has a linear relationship with respect to $\xi$ since $[C]$ is a nonsingular matrix of constant coefficients and $D_1$ in (55) has a linear relationship with respect to $\xi$. In addition, the general solution $\{\Psi\}$ to (68) can be assumed to carry the form:

$$\{\Psi\} = \{\Psi_0\}\exp(\lambda\xi), \tag{71}$$

where $\lambda$ and $\{\Psi_0\}$ are respectively the eigenvalue and eigenvector of the characteristic equation corresponding to (68):

$$\lambda^4[A]\{\Psi_0\} + \lambda^2[B]\{\Psi_0\} + \{C\}\{\Psi_0\} = \{0\}. \tag{72}$$

The above eigenvalue problem can be converted to a generalized eigenvalue problem:

$$\begin{bmatrix} I & 0 \\ 0 & A \end{bmatrix} \begin{Bmatrix} \Psi_0 \\ \Psi_1 \end{Bmatrix} = -\lambda^{-2} \begin{bmatrix} 0 & -I \\ C & B \end{bmatrix} \begin{Bmatrix} \Psi_0 \\ \Psi_1 \end{Bmatrix}, \tag{73}$$

where

$$\{\Psi_1\} = \lambda^2 \{\Psi_0\}. \tag{74}$$

The eigenvalue problem (72) can be solved by using standard, robust, efficient numerical algorithms available in the literature, (e.g., the eig( ) function offered by Matlab™). Consequently, the general solution (67) can be expressed as

$$\{\Phi\} = \sum_{k=1}^{4} [c_k \{\Psi_0^k\} \exp(\lambda_k \xi) + d_k \{\Psi_0^k\} \exp(-\lambda_k \xi)] + \{\Phi_0(\xi)\}. \tag{75}$$

In the above, $\{\Psi_0^k\} (k = 1, 2, 3, 4)$ are the eigenvectors relating the corresponding eigenvalues $\lambda_k (k = 1, 2, 3, 4)$, respectively; $c_k$ and $d_k (k = 1, 2, 3, 4)$ are the real or complex coefficients to be determined to satisfy the traction BCs (8)-(20), which can be reduced into eight linearly independent traction BCs:

$$F(0) = 0, \tag{76}$$

$$F(L / h_2) = -1, \tag{77}$$

$$F'(0) = 0, \tag{78}$$

$$F'(L / h_2) = 0, \tag{79}$$

$$G(0) = 0, \tag{80}$$

$$G(L / h_2) = M_1 / (p_0 h_2^2) + t_0 / p_0 (L / h_2) - h_{12} / 2, \tag{81}$$

$$G'(0) = 0, \tag{82}$$

$$G'(L / h_2) = t_0 / p_0. \tag{83}$$

Consequently, substitution of (75) associated with (70) into (76)-(83) yields a set of eight linear algebraic equations:

$$\sum_{k=1}^{4} c_k \Psi_0^{k,1} + \sum_{k=1}^{4} d_k \Psi_0^{k,1} = -\Phi_0^{(1)}(0), \tag{84}$$

$$\sum_{k=1}^{4} c_k \Psi_0^{k,1} \exp(\lambda_k L/h_2) + \sum_{k=1}^{4} d_k \Psi_0^{k,1} \exp(-\lambda_k L/h_2) = -[1 + \Phi_0^{(1)}(L/h_2)], \tag{85}$$

$$\sum_{k=1}^{4} c_k \lambda_k \Psi_0^{k,1} - \sum_{k=1}^{4} d_k \lambda_k \Psi_0^{k,1} = -\frac{d\Phi_0^{(1)}}{d\xi}, \tag{86}$$

$$\sum_{k=1}^{4} c_k \lambda_k \Psi_0^{k,1} \exp(\lambda_k L / h_2) - \sum_{k=1}^{4} d_k \lambda_k \Psi_0^{k,1} \exp(-\lambda_k L / h_2) = -\frac{d\Phi_0^{(1)}}{d\xi}, \tag{87}$$

$$\sum_{k=1}^{4} c_k \Psi_0^{k,2} + \sum_{k=1}^{4} d_k \Psi_0^{k,2} = -\Phi_0^{(2)}(0), \tag{88}$$

$$\sum_{k=1}^{4} c_k \Psi_0^{k,2} \exp(\lambda_k L / h_2) + \sum_{k=1}^{4} d_k \Psi_0^{k,2} \exp(-\lambda_k L / h_2)$$

$$= M_1 / (p_0 h_2^2) + t_0 / p_0 (L / h_2) - h_{12} / 2 - \Phi_0^{(2)}(L / h_2), \tag{89}$$

$$\sum_{k=1}^{4} c_k \lambda_k \Psi_0^{k,2} - \sum_{k=1}^{4} d_k \lambda_k \Psi_0^{k,2} = -\frac{d\Phi_0^{(2)}}{d\xi}, \tag{90}$$

$$\sum_{k=1}^{4} c_k \lambda_k \Psi_0^{k,2} \exp(\lambda_k L / h_2) - \sum_{k=1}^{4} d_k \lambda_k \Psi_0^{k,2} \exp(-\lambda_k L / h_2) = t_0 / p_0 - \frac{d\Phi_0^{(2)}}{d\xi}. \tag{91}$$

In the above, $\Psi_0^{k,1}$ and $\Psi_0^{k,2}(k = 1, 2, 3, 4)$ are respectively the first and second elements of the $k$-th eigenvector; $\Phi_0^{(1)}$ and $\Phi_0^{(2)}$ are the 1st and 2nd elements of the particular solution vector $\{\Phi_0\}$, respectively. In addition, in the case of thermomechanical stress analysis of the joints due to a pure temperature change, the right terms of (77), (81), and (83) should be set as zero. Accordingly, such modification will further influence the right terms of (85), (89), and (91). Once coefficients $c_k(k = 1, 2, 3, 4)$ and $d_k(k = 1, 2, 3, 4)$ are determined by solving the above set of linear algebraic equations (84)-(91) numerically, relations (44), (45), and (75) finally determine $f$ and $g$ as

$$f(x)/p_0 = \sum_{k=1}^{4} c_k \Psi_0^{k,1} \lambda_k \exp(\lambda_k x / h_2) - \sum_{k=1}^{4} d_k \Psi_0^{k,1} \lambda_k \exp(-\lambda_k x / h_2) + \frac{d\Phi_0^{(1)}}{d\xi}, \tag{92}$$

$$g(x)/p_0 = \sum_{k=1}^{4} c_k \Psi_0^{k,2} \lambda_k^2 \exp(\lambda_k x / h_2) + \sum_{k=1}^{4} d_k \Psi_0^{k,2} \lambda_k^2 \exp(-\lambda_k x / h_2). \tag{93}$$

With the interfacial stress functions $f$ and $g$ available from (92) and (93), all the stress components in the two adherends can be determined according to the stress expressions formulated in Subsection 2.3. By comparison with those obtained by Wu and his co-workers [44], it can be found that the specific type of bonded two-adherend joint only specifies the traction BCs of the joint, which only influence the right terms of (84)-(91). This demonstrates the universal treatment of bonded joints based on proposed variational stress-function method.

## 3. Model Validation and Discussions

### 3.1. Interfacial stresses in a bonded single-lap joint free of shear-force

The present variational stress-function method for stress analysis of bonded single-lap joints is a generalized version based preliminarily on that for side-bonded strap-joints [43-46]. Thus, in the limiting case that the shear-force is ignored, (i.e., $t_0 = 0$) such as a cantilevered single-lap joint subjected to axial tension as illustrated in Figure 3(a), all the derivations formulated in this work will be automatically reduced to those of the single-sided strap joint model [43-46]. Since the accuracy of interfacial stresses predicted by the latter model in the cases of axial tension and pure temperature change has been validated carefully by our recent FEM simulations and other results available in the literature [44-46]. Such study has demonstrated the validity of the present model in the specific mechanical and thermomechanical loading cases.

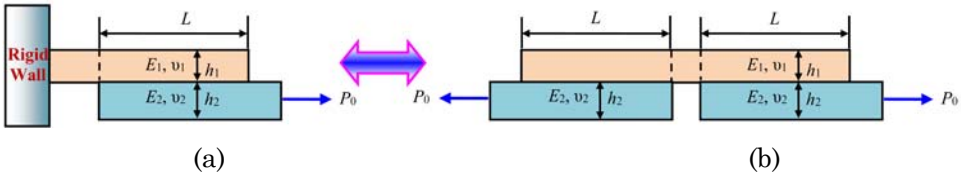


**Figure 3.** Static equivalency between (a) a cantilevered single-lap joint and (b) a side-bonded strap joint subjected to axial tension.

### 3.2. Interfacial stresses in bonded single-lap joints under shear and bending

Within the present theoretical framework, the adherends of the joint model are assumed to be homogeneous, isotropic, linearly elastic solids and under small deformation/deflection. Thus, method of superposition can be safely used to analyze the interfacial stresses of single-lap joints under combined loadings of tension, shearing, bending, and uniform

temperature change, i.e., the interfacial stresses can be determined as the sum of those based on the external loads one by one. Since the interfacial stresses induced by axial tension and uniform temperature change have been studied in our recent study [43-46], herein, the present single-lap joint model was employed to determine the interfacial stresses of a single-lap joint induced by a shear-load (see Figure 4); FEA based on a commercial FEM package (ANSYS™) was conducted to validate the model results. The single-lap joint was assumed being made of a steel plate as the upper adherend ($E_1$ = 210GPa, $\upsilon_1$ = 0.293) and an aluminum plate as the lower adherend ($E_2$ = 70GPa, $\upsilon_2$ = 0.34). The adherends had the same width, other geometries of the joint were: $h_1$ = 2mm (steel), $h_2$ = 4mm (aluminum), and $L$ = 20mm (see Figure 4). The average shear traction of the lower adherend was assumed as $t_0$ = 1MPa being applied at the right end. During the FEM simulation of the interfacial stresses, four-node plane-stress element (PLANE182) and mapped uniform quadrilateral meshes were utilized. Furthermore, due to the specific configuration of the joint, stress singularity exists at the free-edges of the joint. In an attempt to demonstrate the singular stresses near the edges, four mesh sizes, (i.e., $0.4 \times 0.4$mm, $0.2 \times 0.2$mm, $0.1 \times 0.1$mm, and $0.05 \times 0.05$mm) were considered sequentially in the FEM simulations. The interfacial shear and normal (peeling) stresses along the bonding line are plotted in Figures 5(a) and 5(b). It can be found from Figure 5 that the interfacial stresses based on the present variational stress-function method predict the stress variations close to those based on detailed FEM simulations. The shear-stresses predicted by the present method can satisfy the shear-free conditions at the adherend ends while the present FEM results do not. Also, it can be observed that both the maximum interfacial shear and normal stresses appear at the left end of the joint adherend due to the maximum bending moment induced by the shear-force at this end. Herein, it needs to be

mentioned that since the bonding line of the joint is not located along the effective neutral axis of the joint, the bending moment also induces a significant shear-stress along the bonding line which is responsible for the maximum shear-stress at the left end. Thus, interfacial debonding failure mostly appears first at the left edge of the adherends.

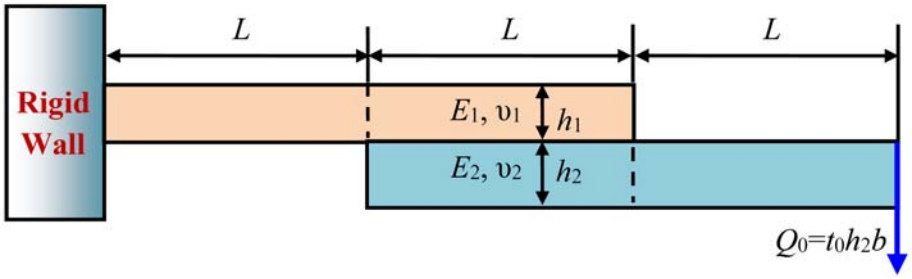


**Figure 4.** Configuration of a cantilevered single-lap joint subjected to a vertical shear-force $Q_0$.

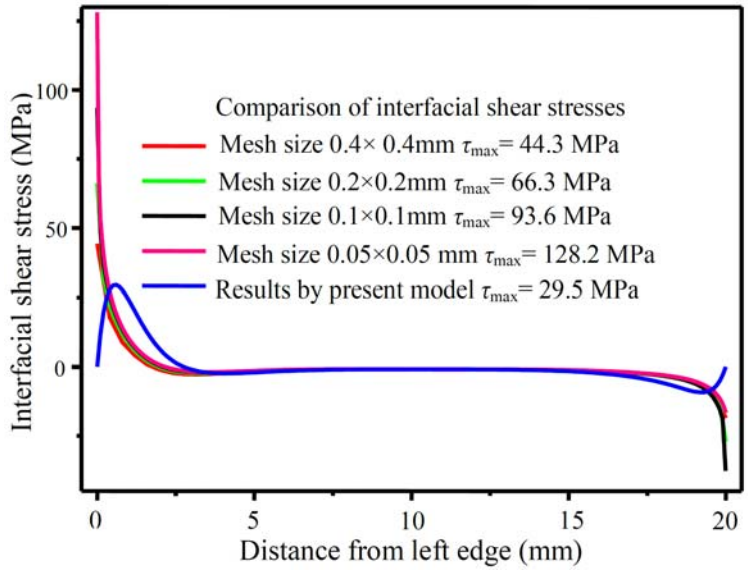


(a)

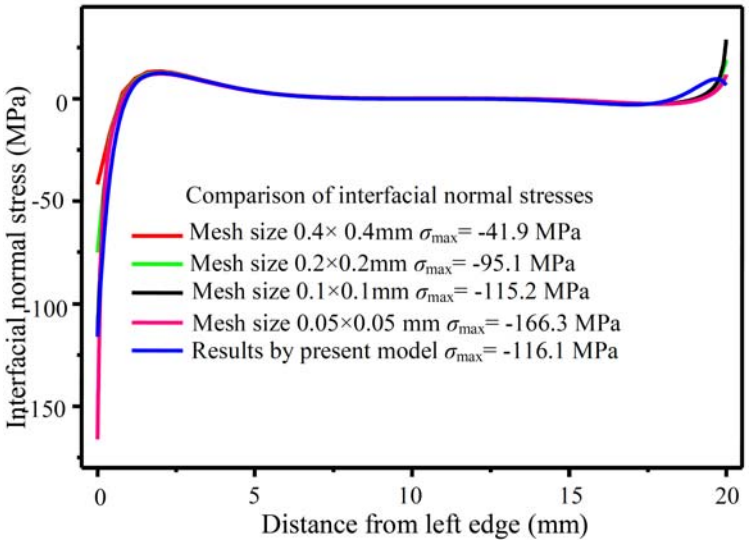


(b)

**Figure 5.** Variations of the interfacial shear and normal stresses in a bonded single-lap joint subjected to a shear-force: (a) interfacial shear-stress and (b) interfacial normal stress.

Furthermore, the present semi-analytic method based on a limited number of eigenfunctions exhibits some deviation on the shear-stress prediction compared to those of the FEM simulations; however, it demonstrates a very high accuracy on the normal stress prediction. Moreover, due to existence of the singular stress-field near the adherend ends, theoretically, the normal stress will tend to infinity at the free edge. Thus, the interfacial stresses predicted by the FEA tend to be larger and larger with the finer meshes to be considered as demonstrated in Figure 5. Like most joint models available in the literature, the present method is unable to predict such stress singularity. However, the present method has demonstrated a very good fitting to the interfacial stress variations predicted by using FEM that confirms the validity of the present method.

### 3.3. Scaling analysis of interfacial stresses due to mechanical loads

This section is designated to examine the effects of adherend material properties and geometries on the interfacial stress variation of the bonded single-lap joint as shown in Figure 4, i.e., scaling analysis. Such scaling analysis of interfacial stresses can provide an explicit understanding of the dependency of joint interfacial stresses upon materials and geometries of the adherends, which is particularly useful to joint design and failure analysis. In the analysis, five thickness ratios ($h_1/h_2$ = 0.2, 0.5, 1, 2, 5), two length ratios ($L/h_2$ = 5, 10), and two modulus ratios ($E_1/E_2$ = 3, 10) are used; Poisson's ratios of the adherends are fixed as $\upsilon_1$ = 0.293 and $\upsilon_2$ = 0.345. The bonded single-lap joint is considered in *plane-strain* state and loaded by a single shear-force with the average shear-stress $t_0$ across the cross-section as shown in Figure 4. Due to the importance of the interfacial normal stress in strength analysis of such joints, the scaling analysis below only considers variation of the normal stress.

Figure 6 show variations of the dimensionless interfacial normal (peeling) stress $\sigma / t_0$ with the dimensionless distance $x / h_2$ from the left adherend-end at varying length, thickness, and modulus ratios, respectively. It can be observed that for given overlap length ratio $(L / h_2)$ (see Figure 4), the maximum normal stress at the left adherend-end decreases rapidly with the increase of either the thickness ratio $(h_1 / h_2)$ or modulus ratio $(E_1 / E_2)$; however, the maximum normal stress at the right adherend-end varies in the opposite tendency to that of the left adherend-end. This can be explained such that the bending moment induced by the shear-force is located at the left end of the upper adherend and at the right end of the lower adherend; as a result, the normal stress decreases with increasing moment inertia of the adherend cross-sectional area which has a cubic relationship with the thickness ratio $(h_1 / h_2)$ and a linear relationship with the modulus ratio $(E_1 / E_2)$. Furthermore, such variations will be further enhanced with the increase of the length ratio $(L / h_2)$ because the larger the length ratio $(L / h_2)$ is, the larger is the bending moment to be induced. Therefore, the scaling analysis of interfacial stresses can clearly indicate the stress dependency upon the material properties, geometries, and external loads. Such scaling analysis can be further extended to consider the effect of combined loads including mechanical and thermomechanical loads, among others.

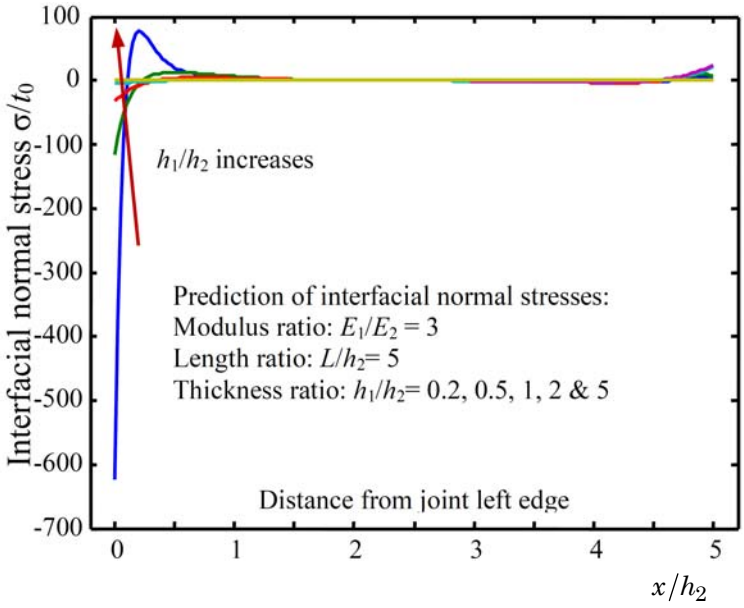
Interfacial normal stress σ/$t_0$
100
0
-100
-200
-300
-400
-500
-600
-700
$h_1/h_2$ increases
Prediction of interfacial normal stresses:
Modulus ratio: $E_1/E_2$ = 3
Length ratio: $L/h_2$= 5
Thickness ratio: $h_1/h_2$= 0.2, 0.5, 1, 2 & 5
Distance from joint left edge
0
1
2
3
4
5
$x/h_2$

(a)

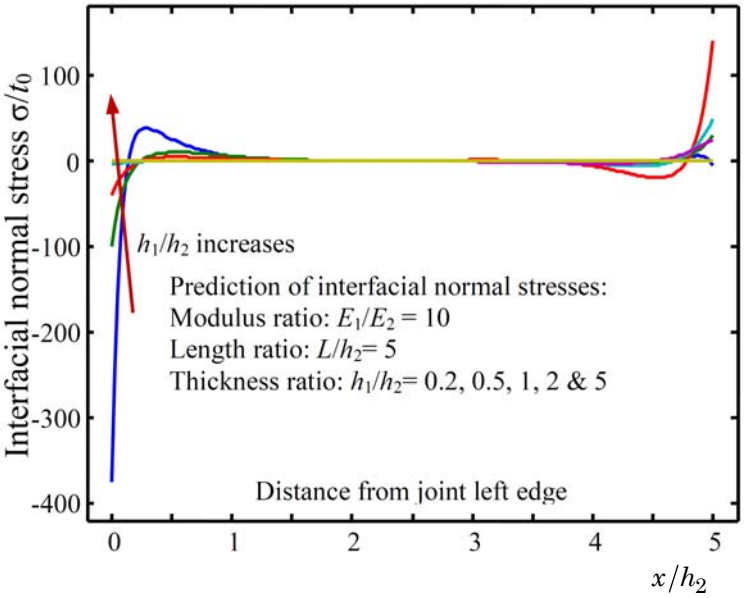
Interfacial normal stress σ/$t_0$
100
0
-100
-200
-300
-400
$h_1/h_2$ increases
Prediction of interfacial normal stresses:
Modulus ratio: $E_1/E_2$ = 10
Length ratio: $L/h_2$= 5
Thickness ratio: $h_1/h_2$= 0.2, 0.5, 1, 2 & 5
Distance from joint left edge
0
1
2
3
4
5
$x/h_2$

(b)

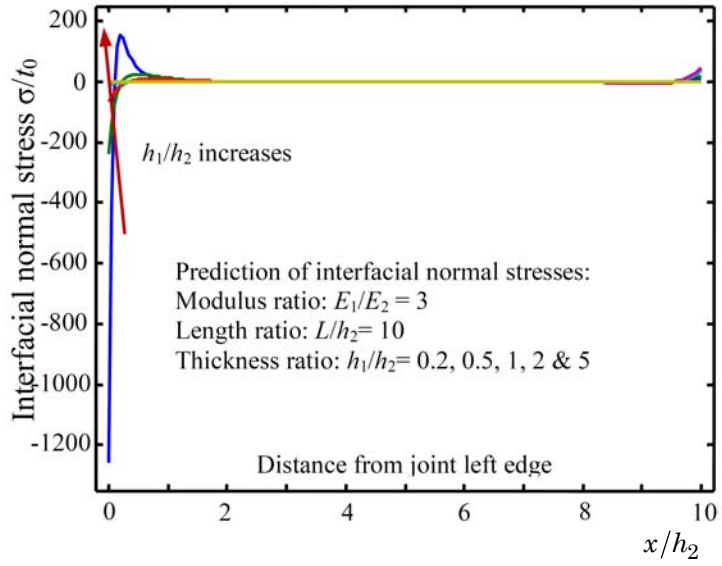


(c)

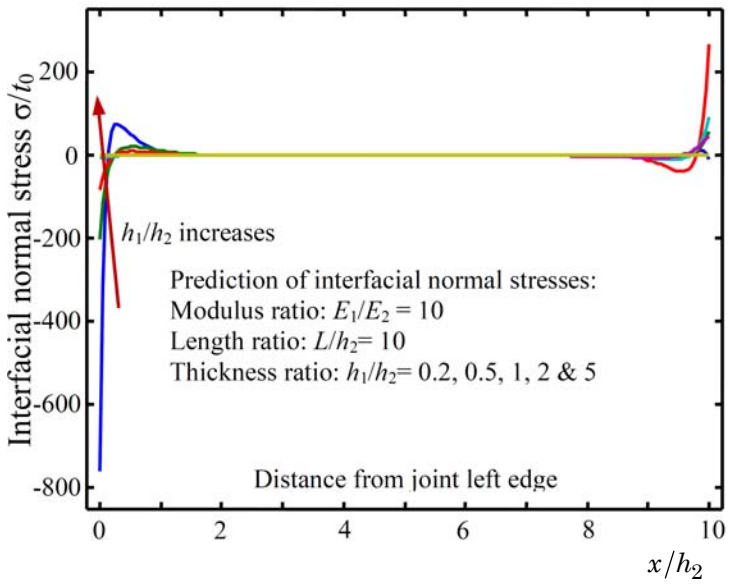


(d)

**Figure 6.** Variations of the dimensionless interfacial normal stress in bonded single-lap joints with the dimensionless distance from the right adherend-end at varying thickness, modulus, and length ratios.

## 4. Concluding Remarks

The stress-function variational method has been extended successfully for determining the interfacial stresses of bonded single-lap joints subjected to mechanical and thermomechanical loads. During the process, the axial normal stress was assumed to vary linearly in the adherend cross-sections of the joints; the statically compatible in-plane shear and transverse normal stresses were determined to vary parabolically and cubically in the adherend cross-sections, respectively. Two coupled governing ODEs of constant coefficients have been formulated successfully, which can be regarded as universal for stress analysis of a variety of bonded two-adherend joints with varying traction BCs to correspond to specific bonded joints of interest. The joint model generalized in this study is capable of providing reliable stress variation in bonded joints useful to joint design, structural optimization, and strength evaluation. The theoretical merits of the present formulation include that all the traction BCs are satisfied exactly and all the material and geometrical parameters have been rationally integrated into the model. The numerical process corresponding to the present joint model is self-consistent, robust, and efficient.

The joint model formulated in the present work provides an efficient, powerful, theoretical tool to understand the scaling behaviour of the entire stress field in bonded joints, especially the variation of the debonding stresses along the bonding lines. The present formalism can be conveniently generalized for developing novel, efficient and reliable joint models for stress and strength analysis of adhesively bonded multi-material and composite joints where knowledge of interfacial and interlaminar stresses plays a critical role to understand their strength and durability and to improve the relevant structural design and manufacturing.

**Acknowledgements**

Partial support of this work by the Centennial Endowment Fund of NDSU Development Foundation and the NDSU Faculty Research Initiative Grant is gratefully appreciated.

## References

[1] O. Volkersen, Die Nietkraftverteilung in zugbeanspruchten Nietverbindungen mit konstanten Laschenquerschnitten, Luftfarhtforschung 15 (1938), 41-47.

[2] M. Goland and E. Reissner, The stresses in cemented joints, Journal of Applied Mechanics-Transactions of ASME 11(1) (1944), 17-27.

[3] L. F. M. da Silva, P. J. C. das Neves, R. D. Adams and J. K. Spelt, Analytic models of adhesively bonded joints-part I: Literature survey, International Journal of Adhesion and Adhesives 29(3) (2009), 319-330.

DOI: https://doi.org/10.1016/j.ijadhadh.2008.06.005

[4] L. F. M. da Silva, P. J. C. das Neves, R. D. Adams, A. Wang and J. K. Spelt, Analytic models of adhesively bonded joints-part II: Comparative study, International Journal of Adhesion and Adhesives 29(3) (2009), 331-341.

DOI: https://doi.org/10.1016/j.ijadhadh.2008.06.007

[5] L. J. Hart-Smith, Adhesive-Bonded Single-Lap Joints, NASA, CR-112236, 1973.

[6] L. J. Hart-Smith, Adhesive-Bonded Double-Lap Joints, NASA, CR-112235, 1973.

[7] F. Erdogan and M. Ratwani, Stress distribution in bonded joints, Journal of Composite Materials 5(3) (1971), 378-393.

DOI: https://doi.org/10.1177/002199837100500308

[8] F. Delale, F. Erdogan and M. N. Aydinoglu, Stress in adhesively bonded joints: A closed-form solution, Journal of Composite Materials 15(3) (1981), 249-271.

DOI: https://doi.org/10.1177/002199838101500305

[9] D. Chen and S. Cheng, An analysis of adhesive-bonded single-lap joints, Journal of Applied Mechanics 50(1) (1983), 109-115.

DOI: https://doi.org/10.1115/1.3166976

[10] D. Chen and S. Cheng, Stress distribution in plane scarf and butt joints, Journal of Applied Mechanics 57(1) (1990), 78-83.

DOI: https://doi.org/10.1115/1.2888327

[11] D. Chen and S. Cheng, Torsional stress in tubular lap joints, International Journal of Solids and Structures 29(7) (1992), 845-853.

DOI: https://doi.org/10.1016/0020-7683(92)90020-T

[12] X.-F. Wu, Y. A. Dzenis and K. W. Strabala, Free-edge stresses and progressive cracking in surface coatings of circular torsion bars, International Journal of Solids and Structures 45(7-8) (2008), 2251-2264.

DOI: https://doi.org/10.1016/j.ijsolstr.2007.11.020

[13] N. Pugno and A. Carpinteri, Tubular adhesive joints under axial load, Journal of Applied Mechanics 70(6) (2003), 832-839.

DOI: https://doi.org/10.1115/1.1604835

[14] O. Nemes, F. Lachaud and A. Mojtabi, Contribution to the study of cylindrical adhesive joining, International of Journal of Adhesion and Adhesives 26(6) (2006), 474-480.

DOI: https://doi.org/10.1016/j.ijadhadh.2005.07.009

[15] O. Nemes and F. Lachaud, Modeling of cylindrical adhesively bonded joints, Journal of Adhesion Science and Technology 23(10-11) (2009), 1383-1393.

DOI: https://doi.org/10.1163/156856109X432983

[16] T. Sekercioglu, Strength based reliability of adhesively bonded tubular lap joints, Materials and Design 28(6) (2007), 1914-1918.

DOI: https://doi.org/10.1016/j.matdes.2006.04.004

[17] S. Kumar, Analysis of tubular adhesive joints with a functionally modulus graded bondline subjected to axial loads, International Journal of Adhesion and Adhesives 29(8) (2009), 785-795.

DOI: https://doi.org/10.1016/j.ijadhadh.2009.06.006

[18] C. Yang and Z. D. Guan, Stress analysis of composite pipe joints under combined torsional and tensile loading, Journal of Pressure Vessel Technology 131(5) (2009); Article 051210.

DOI: https://doi.org/10.1115/1.3151810

[19] B. A. Bednarcyk, J. Zhang, C. S. Collier, Y. Bansal and M. J. Pindera, Analysis tools for adhesively bonded composite joints, Part 1: Higher-order theory, AIAA Journal 44(1) (2006), 171-180.

DOI: https://doi.org/10.2514/1.12061

[20] Q. T. Luo and L. Y. Tong, Closed form solutions for nonlinear analysis of single-sided bonded composite patch repairs, AIAA Journal 45(12) (2007), 2957-2965.

DOI: https://doi.org/10.2514/1.30108

[21] Q. T. Luo and L. Y. Tong, Analytical solutions for nonlinear analysis of composite single-lap adhesive joints, International Journal of Adhesion and Adhesives 29(2) (2009), 144-154.

DOI: https://doi.org/10.1016/j.ijadhadh.2008.01.007

[22] J. J. Radice and J. R. Vinson, On the analysis of adhesively bonded structures: A high order semi-elastic adhesive layer model, Composites Science and Technology 68(2) (2008), 376-386.

DOI: https://doi.org/10.1016/j.compscitech.2007.06.024

[23] Z. S. Wu, H. Yuan and H. D. Niu, Stress transfer and fracture propagation in different kinds of adhesive joints, Journal of Engineering Mechanics 128(5) (2002), 562-573.

DOI: https://doi.org/10.1061/(ASCE)0733-9399(2002)128:5(562)

[24] H. Yuan, J. G. Teng, R. Seracino, Z. S. Wu and J. Yao, Full-range behavior of FRP-to-concrete bonded joints, Engineering Structures 26(5) (2004), 553-565.

DOI: https://doi.org/10.1016/j.engstruct.2003.11.006

[25] K. Leffler, K. S. Alfredsson and U. Stigh, Shear behaviour of adhesive layers, International Journal of Solids and Structures 44(2) (2007), 530-545.

DOI: https://doi.org/10.1016/j.ijsolstr.2006.04.036

[26] A. Carpinteri, P. Cornetti and N. Pugno, Edge debonding in FRP strengthened beams: Stress versus energy failure criteria, Engineering Structures 31(10) (2009), 2436-2447.

DOI: https://doi.org/10.1016/j.engstruct.2009.05.015

[27] A. J. Curley, H. Hadavinia, A. J. Kinloch and A. C. Taylor, Predicting the service-life of adhesively-bonded joints, International Journal of Fracture 103(1) (2000), 41-69.

DOI: https://doi.org/10.1023/A:1007669219149

[28] F. Mortensen and O. T. Thomsen, Analysis of adhesive bonded joints: A unified approach, Composites Science and Technology 62(7-8) (2002), 1011-1031.

DOI: https://doi.org/10.1016/S0266-3538(02)00030-1

[29] C. D. M. Liljedahl, A. D. Crocombe, M. A. Wahab and I. A. Ashcroft, Damage modelling of adhesively bonded joints, International Journal of Fracture 141(1-2) (2006), 147-161.

DOI: https://doi.org/10.1007/s10704-006-0072-9

[30] M. Quaresimin and M. Ricotta, Fatigue behaviour and damage evolution of single lap bonded joints in composite material, Composites Science and Technology 66(2) (2006), 176-187.

DOI: https://doi.org/10.1016/j.compscitech.2005.04.026

[31] C.-S. Ban, Y. H. Lee, J.-H. Choi and J.-H. Kweon, Strength prediction of adhesive joints using the modified damage zone theory, Composite Structures 86(1-3) (2008), 96-100.

DOI: https://doi.org/10.1016/j.compstruct.2008.03.016

[32] P. A. Gustafson and A. M. Wass, The influence of adhesive constitutive parameters in cohesive zone finite element models of adhesively boned joints, International Journal of Solid and Structures 46(10) (2009), 2201-2215.

DOI: https://doi.org/10.1016/j.ijsolstr.2008.11.016

[33] J. Q. Cheng and F. Taheri, A novel smart adhesively bonded joint system, Smart Materials and Structures 14(5) (2005), 971-981.

DOI: https://doi.org/10.1088/0964-1726/14/5/035

[34] J. Q. Cheng, F. Taheri and H. P. Han, Strength improvement of a smart adhesive bonded joint system by partially integrated piezoelectric patches, Journal of Adhesion Science and Technology 20(6) (2006), 503-518.

DOI: https://doi.org/10.1163/156856106777213285

[35] J. W. Kwon, W. S. Chin and D. G. Lee, Piezoelectric monitoring of the reliability of adhesive joints, Journal of Adhesion Science and Technology 17(6) (2003), 777-796.

DOI: https://doi.org/10.1163/156856103321645158

[36] J. Q. Cheng, X. X. Wu, G. Q. Li, F. Taheri and S. S. Pang, Development of a smart composite pipe joint integrated with piezoelectric layers under tensile loading, International of Journal of Solids and Structures 43(17) (2006), 5370-5385.

DOI: https://doi.org/10.1016/j.ijsolstr.2006.01.001

[37] M. A. Khan, S. Kumar and J. N. Reddy, Material-tailored adhesively bonded multilayers: A theoretical analysis, International Journal of Mechanical Sciences 148 (2018), 246-262.

DOI: https://doi.org/10.1016/j.ijmecsci.2018.08.017

[38] R. Hadj-Ahmed, G. Foret and A. Ehrlacher, Stress analysis in adhesive joints with a multiparticle model of multilayered materials (M4), International Journal of Adhesion and Adhesives 21(4) (2001), 297-307.

DOI: https://doi.org/10.1016/S0143-7496(00)00034-8

[39] A. D. Diaz, R. Hadj-Ahmed, G. Foret and A. Ehrlacher, Stress analysis in a classical double lap, adhesively bonded joint with a layerwise model, International Journal of Adhesion and Adhesives 29(1) (2009), 67-76.

DOI: https://doi.org/10.1016/j.ijadhadh.2008.01.004

[40] S. A. Yousefsani and M. Tahani, Accurate determination of stress distribution in adhesively bonded homogeneous and heterogeneous double-lap joints, European Journal of Mechanics A 39 (2013), 197-208.

DOI: https://doi.org/10.1016/j.euromechsol.2012.12.001

[41] S. A. Yousefsani and M. Tahani, Analytic solutions for adhesively bonded composite single-lap joints under mechanical loadings using full layerwise theory, International Journal of Adhesion and Adhesives 43 (2013), 32-41.

DOI: https://doi.org/10.1016/j.ijadhadh.2013.01.012

[42] S. A. Yousefsani and M. Tahani, Edge effects in adhesively bonded composite joint integrated with piezoelectric patches, Composite Structures 200 (2018), 187-194.

DOI: https://doi.org/10.1016/j.compstruct.2018.05.071

[43] X.-F. Wu and R. A. Jenson, Semianalytic stress-function variational approach for the interfacial stresses in bonded joints, Journal of Engineering Mechanics 140(11) (2014), 04014089.

DOI: https://doi.org/10.1061/(ASCE)EM.1943-7889.0000803

[44] X.-F. Wu and R. A. Jenson, Stress-function variational method for stress analysis of bonded joints under mechanical and thermal loads, International Journal of Engineering Science 49(3) (2011), 279-294.

DOI: https://doi.org/10.1016/j.ijengsci.2010.11.005

[45] X.-F. Wu and Y. H. Zhao, Stress-function variational method for interfacial stress analysis of adhesively bonded joints, International Journal of Solids and Structures 50(25-26) (2013), 4305-4319.

DOI: https://doi.org/10.1016/j.ijsolstr.2013.09.002

[46] X.-F. Wu, R. A. Jenson and Y. H. Zhao, Stress-function variational approach to the interfacial stresses and progressive cracking in surface coatings, Mechanics of Materials 69(1) (2014), 195-203.

DOI: https://doi.org/10.1016/j.mechmat.2013.10.004

[47] Z. G. Suo and J. W. Hutchinson, Interface crack between two elastic layers, International Journal of Fracture 43(1) (1990), 1-18.

DOI: https://doi.org/10.1007/BF00018123

[48] J. W. Hutchinson and Z. G. Suo, Mixed mode cracking in layered materials, Advance in Applied Mechanics 29 (1991), 63-191.

DOI: https://doi.org/10.1016/S0065-2156(08)70164-9

[49] H.-H. Yu, M. Y. He and J. W. Hutchinson, Edge effects in thin film delamination, Acta Materialia 49(1) (2001), 93-107.

DOI: https://doi.org/10.1016/S1359-6454(00)00293-7

[50] X.-F. Li, Closed-form solution for a mode-III interface crack between two bonded dissimilar elastic layers, International Journal of Fracture 109(2) (2001), 3-8.

DOI: https://doi.org/10.1023/A:1010960305812

[51] X.-F. Wu and Y. A. Dzenis, Closed-form solution for a mode-III interfacial edge crack between two bonded dissimilar elastic strips, Mechanics Research Communications 29(5) (2002), 407-412.

DOI: https://doi.org/10.1016/S0093-6413(02)00317-8

[52] X.-F. Wu, E. Lilla and W.-S. Zou, A semi-infinite crack between two bonded dissimilar elastic strips, Archive of Applied Mechanics 72(8) (2002), 630-636.

DOI: https://doi.org/10.1007/s00419-002-0240-y

[53] H.-H. Yu and J. W. Hutchinson, Delamination of thin film strips, Thin Solid Films 423(1) (2003), 54-63.

DOI: https://doi.org/10.1016/S0040-6090(02)00973-2

[54] X.-F. Wu, Y. A. Dzenis and W.-S. Zou, Interfacial edge crack between two bonded dissimilar orthotropic strips under antiplane point loading, Zeitschrift fur Angewandte Mathematik und Mechanik 83(6) (2003), 419-422.

DOI: https://doi.org/10.1002/zamm.200310063

[55] X.-F. Wu, Y. A. Dzenis and T.-Y. Fan, Two semi-infinite interfacial cracks between two bonded dissimilar elastic strips, International of Journal of Engineering Science 41(55) (2003), 1699-1710.

DOI: https://doi.org/10.1016/S0020-7225(03)00107-1

[56] X.-F. Wu, Y. A. Dzenis and E. Gokdag, Edge-cracked orthotropic bimaterial butt joint under antiplane singularity, International Journal of Nonlinear Science and Numerical Simulation 5(4) (2004), 347-354.

DOI: https://doi.org/10.1515/IJNSNS.2004.5.4.347

[57] X.-F. Li and K. Y. Lee, Closed-form solution for an orthotropic elastic strip with a crack perpendicular to the edges under arbitrary anti-plane shear, Zeitschrift fur Angewandte Mathematik und Mechanik 89(5) (2009), 370-382.

DOI: https://doi.org/10.1002/zamm.200900233

■